New Journal of Physics
The open access journal at the forefront of physics

Deutsche Physikalische Gesellschaft DPG IOP Institute of Physics

Formation of a drop: viscosity dependence of three flow regimes

To cite this article: Alexander Rothert *et al* 2003 *New J. Phys.* **5** 59

View the article online for updates and enhancements.

Related content

- Physics of liquid jets
  Jens Eggers and Emmanuel Villermaux
- Two-dimensional turbulence: a review of some recentexperiments
  Hamid Kellay and Walter I Goldburg
- A new flow focusing technique to produce very thin jets
  A J Acero, N Rebollo-Muñoz, J M Montanero et al.

Recent citations

- Oscillating path between self-similarities in liquid pinch-off
  Antoine Lagarde *et al*
- Effect of soluble surfactants on pinch-off of moderately viscous drops and satellite size
  Nina M. Kovalchuk *et al*
- Pardeep *et al*

IOP ebooks™

Bringing you innovative digital publishing with leading voices to create your essential collection of books in STEM research.

Start exploring the collection - download the first chapter of every title for free.

This content was downloaded from IP address 132.180.25.140 on 21/11/2018 at 16:28

New Journal of Physics
An Institute of Physics and Deutsche Physikalische Gesellschaft Journal

Formation of a drop: viscosity dependence of three flow regimes

Alexander Rothert, Reinhard Richter and Ingo Rehberg
Physikalisches Institut, Experimentalphysik V, Universität Bayreuth, D-95440 Bayreuth, Germany
E-mail: reinhard.richter@uni-bayreuth.de

New Journal of Physics **5** (2003) 59.1–59.13 (http://www.njp.org/)
Received 29 January 2003
Published 6 June 2003

Abstract. We observe the drop pinch-off at a nozzle for different viscosities and investigate three consecutive flow types. In its first stage the neck of the drop shrinks in an accelerated manner similar to the instability of a liquid cylinder. In the vicinity of the pinch point the motion becomes self-similar at a certain time. The self-similar domain consists of two flow regimes separated by a second transition point. The viscosity dependence of the transition points can be described by linear functions. Moreover, it is uncovered that both transitions occur when two different critical neck radii are reached. These radii are found to be independent of viscosity.

Contents

1. Introduction

When observing a dripping faucet in the kitchen-laboratory, for a long time one hardly detects any change, until suddenly the drop has gone. Even from this rough observation one may deduce that for the gross variation in timescale consecutively different flow types are responsible.

PII: S1367-2630(03)58880-2
© IOP Publishing Ltd and Deutsche Physikalische Gesellschaft

The first regime is governed by an accelerated flow similar to that of a liquid cylinder becoming unstable [1]. Whereas it is well accepted that for vertical jet experiments this theory applies [2, 3], Henderson *et al* [4] suggest that it is not appropriate for the slow dynamics at the beginning of droplet formation. They state that the wavenumber is time dependent in this type of experiment. From this they conclude that the dominant mode cannot be described by a simple exponential law. In contrast, Clanet and Lasheras [5] measure the growth rate via the temporal evolution of the neck diameter of a falling drop of water. They show that Rayleigh's theory is valid even in this type of experiment for different nozzle diameters. In the first part of the paper we further investigate the applicability of Rayleigh's theory under variation of the viscosity of a glycerin–water mixture.

Under evolution of the primary instability the classical linear stability analysis breaks down, and one eventually enters the regime of self-similar flow. Here the profile and the flow field follow universal scaling functions, where the time and length scales are determined by the material parameters. Due to its practical implication for the final pinch-off this regime has attracted considerable attention in the recent years [6]. A qualitative experimental presentation of the self-similarity was given by Peregrine *et al* [7].

Actually, one has to subdivide the self-similar flow regime into two different regimes. The case of Stokes flow, i.e. neglecting the influence of inertia, was treated theoretically by Papageorgiou [8]. Experimental evidence for this flow regime was presented in [9]. However, when the necking process reaches the point of pinch-off, inertia can no longer be neglected due to the increasing velocity inside the neck [6]. One enters the regime of inertial–viscous flow. Following Lee [10] a theoretical description based on a one-dimensional approximation of the Navier–Stokes equation was given by Eggers [11]. Experimental agreement with, and comparison with a numerical simulation of, the solution for Navier–Stokes flow was presented in [12] and [13], respectively.

Whereas several experiments have focused on the specific flow regimes, not much attention has been devoted to the transitions between them. A transition between the latter two flow regimes, i.e. from the viscous-dominated to the inertial–viscous flow regime, was demonstrated experimentally in [14]. It remained unresolved how a change of viscosity influences the temporal extension of both regimes. We tackle this question in the second part of the paper and verify both the solution for Stokes flow and the one for Navier–Stokes flow in a certain range of viscosity. Moreover, we investigate how this parameter acts on the transition between the accelerated and the self-similar regime.

2. Experimental setup

In figure 1 the experimental setup is shown. A syringe pump serves for a low and constant flow rate of 0.1 ml min^{-1}. We ensure that only gravity and capillary forces are acting on the falling drop. The syringe is connected via a silicone flexible tube to a Hirschmann pipette tip at whose lower part the drop formation occurs. The outer diameter of the nozzle wetted by the fluid amounts to 1 mm at the orifice. Background illumination is provided with a cold light source diffused by a frosted glass. A high-speed CCD camera (Kodak Ektapro High-Spec Motion Analyser) detects the falling drops with 239×192 pixels of 32×32 μm at record rates between 1000 and 12 000 frames s^{-1}. An objective with a focal distance of 105 mm (60 mm) and an aperture of 37.5 mm (21.4 mm) diameter maps either a whole drop or the vicinity of the neck onto the CCD array with a magnification of 1.5 or 5.2, respectively.

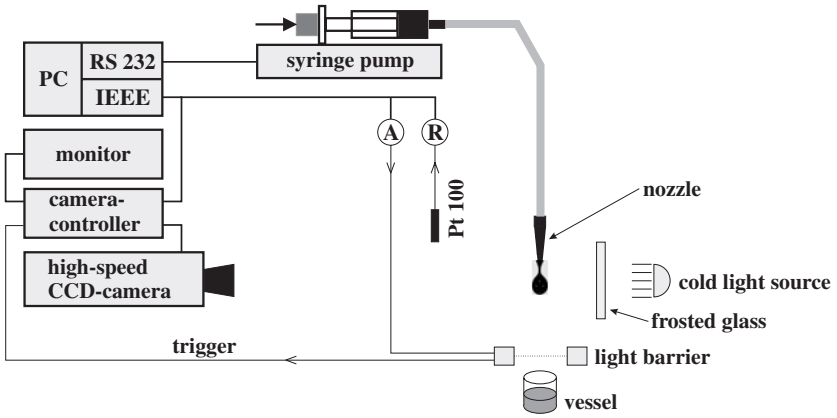

Figure 1. A schematic diagram of the experimental setup.

To guarantee constant initial conditions for successive measurements we use the falling drops to trigger the camera via a light barrier. The frames are stored during the recording in the camera controller and analysed afterwards by digital image processing. The fluid interface is detected as the maximum of the gradient of the image intensity, with an interpolation technique to optimize the spatial resolution.

We use for the experiments glycerin–water mixtures, whose material parameters are changed by varying the mass fraction. By a change of the mass fraction of 100% the surface tension γ varies by 14%, the density ϱ by 26% and the dynamic viscosity η by a factor of 10^3. Thus the viscosity is the most significant parameter. For practical reasons the material parameters were determined from the mass fraction according to the literature. The surface tension can be found in [15], the density in [16] and the dynamic viscosity in [17], respectively. Intermediate values were obtained by fitting a fourth-order polynomial to the logarithmic viscosity and interpolating the surface tension and density with a cubic spline. A cross-check with measured material parameters was successful.

3. Experimental results

Now we proceed with the description of the experimental results. In figure 2 three series of pictures showing the last few milliseconds of the pinch-off process of falling drops are presented. One can see the downward movement and necking of a droplet for different viscosities in rows (a)–(c). The time goes from the left-hand side to the right-hand side, whereas the record rate amounts to 1000 frames s^{-1}. Here only every third frame is shown. The series in figure 2(a) starts in the accelerated flow regime. In the fourth frame the formation of a thin filament can be observed, which is characteristic for the self-similar flow. With growing viscosity the pinch-off process slows down, what can be seen in the smaller neck diameter in the corresponding pictures in the series (b) and (c). Furthermore, the neck becomes longer during the break-off, so that the drop is positioned at a greater distance from the nozzle at the moment of rupture.

A magnification of the region around the neck immediately before and after the pinch-off is shown in figure 3. At a record rate of 12 000 frames s^{-1} one can clearly observe the elongation and thinning of the filament connecting the main drop and the fluid remaining at the nozzle. The timescale of this process becomes longer when viscosity is increased from (a) to (b). We see

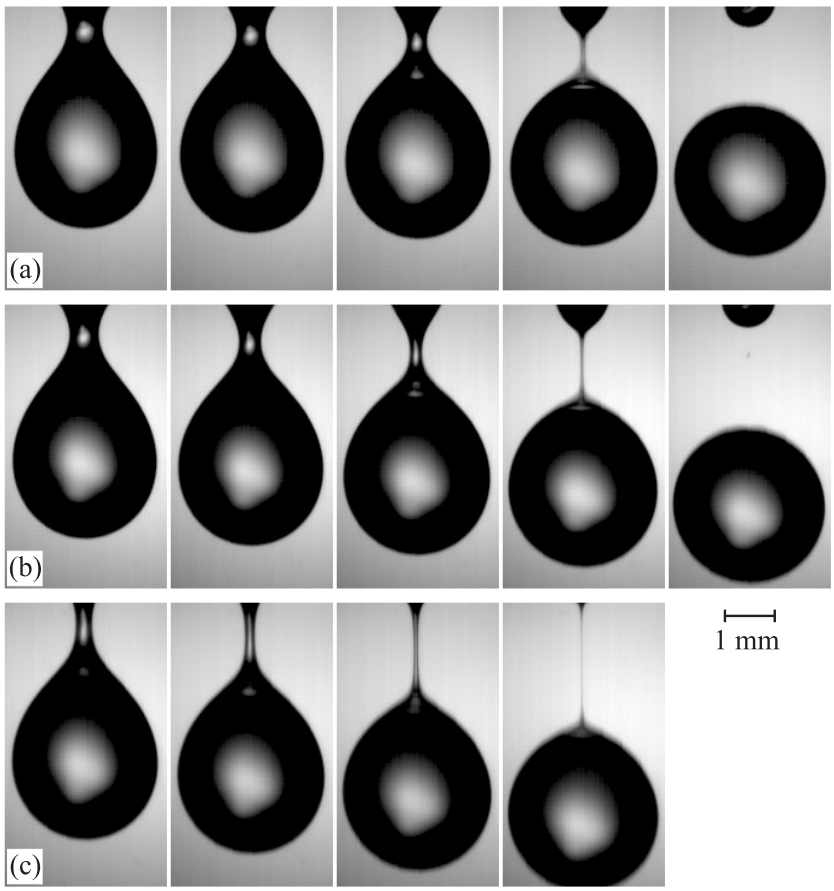

Figure 2. The pinch-off of a falling drop of a glycerin–water mixture for a kinematic viscosity of $\nu = 77.1$ mm^2 s^{-1} (row (a)), $\nu = 126.7$ mm^2 s^{-1} (row (b)) and $\nu = 199.3$ mm^2 s^{-1} (row (c)). The orifice of the nozzle is positioned at the top edge of the frames in (a) and (b), and 0.6 mm above the top edge in (c), respectively. The images in (a)–(c) are recorded at the same times and the time interval amounts to $\Delta t = 3$ ms. For (b) also see animation.

that first the filament separates at its lower end, where it is attached to the drop. After this the filament retracts upwards due to the inertia of the fluid while a second pinch-off on the upper side occurs. Because of the surface tension the filament forms a so-called satellite droplet whose size seems to be decreasing with increasing viscosity.

To quantify the pinch-off process we analyse the drop profile by means of digital image processing and extract the neck radius $h_{\min}$ by fitting a parabola to the vicinity (± 10 pixels) of the minimum. This quantity is plotted in figure 4 as a function of time, where the time t is measured relatively to the point of pinch-off t_0. Starting near the nozzle radius, i.e. $r_0 = 0.5$ mm, the neck shrinks accelerated in the first stage of break-off. By fitting the data with an exponential law we get a good agreement (solid curves in figure 4) for different viscosities. One could estimate the growth rates following from this fit, but in order to prove whether the dispersion relation given by Rayleigh [1] is applicable on drop formation of viscous liquids, we take a more rigorous approach.

First we assume that the drop profile between the nozzle opening and the position $z_{\min}$ of

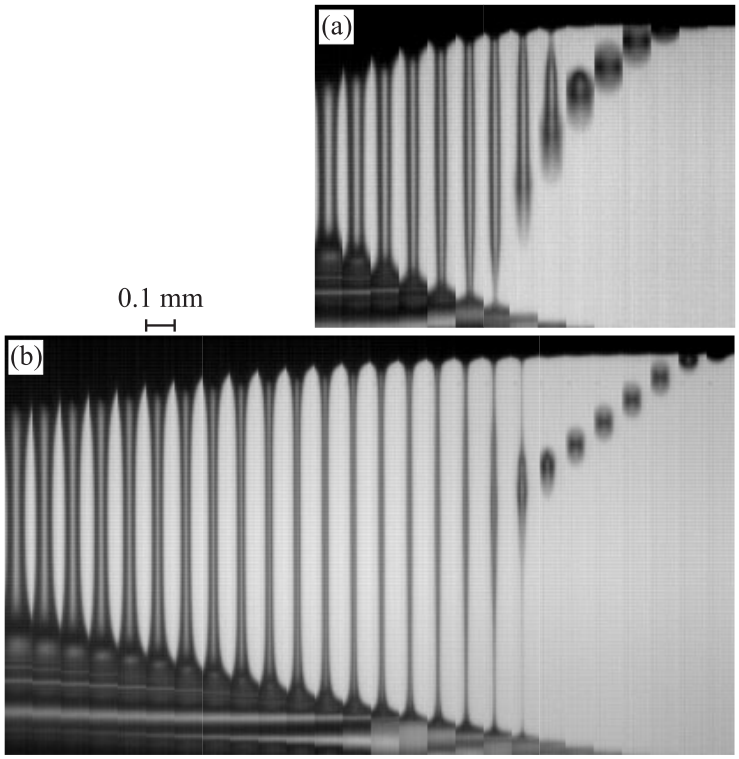

Figure 3. Series of pictures showing the elongation and thinning of the neck and the formation of a satellite droplet after the pinch-off for a viscosity of (a) $\nu = 45.7$ mm^2 s^{-1} (see animation) and (b) $\nu = 82.9$ mm^2 s^{-1} (see animation). The time lap between adjacent frames is $\Delta t = 83$ μs, the scale gives the width of a single image.

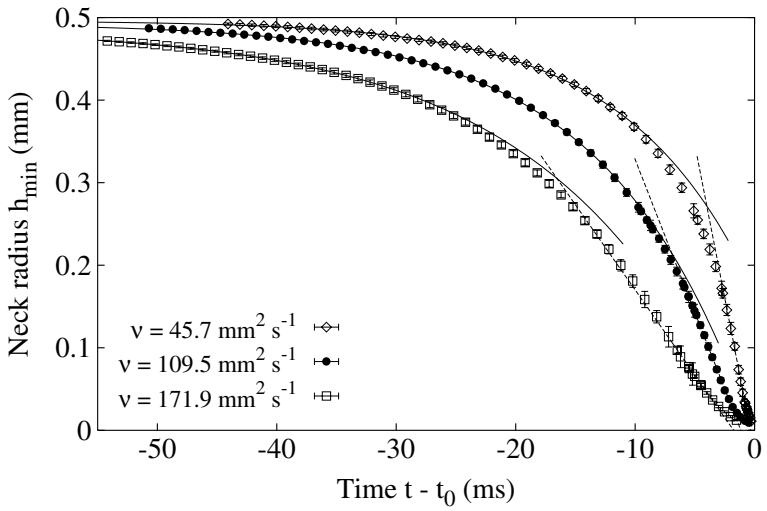

Figure 4. Time evolution of the neck radius for three different viscosities. The solid curves are exponential fits whereas the dashed lines are linear fits according to Stokes flow.

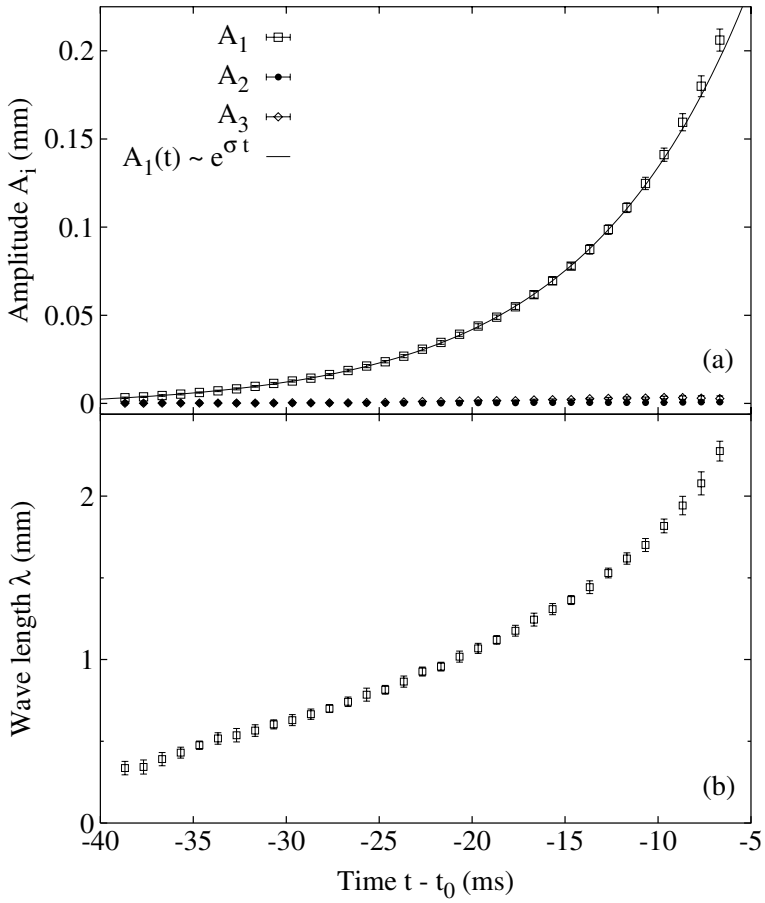

Figure 5. Time evolution of the first three harmonics (a) of the periodic continuation of the profile in the interval $[z_{\text{nozzle}}, z_{\text{min}}]$ and the corresponding wavelength of the dominant mode (b).

the minimum corresponds to the quarter-wavelength of a periodic function. To make a suitable conversion we construct from this segment of the profile a whole period and apply a Fourier transformation on it. Figure 5(a) displays the amplitudes of the first three harmonics, obtained in this way, versus time. We see that the first harmonic is the dominant mode. From this it can be deduced that a part of the profile, i.e. the interval $[z_{\text{nozzle}}, z_{\text{min}}]$ can be described at the beginning of the pinch-off process by a sinusoidal function according to Rayleigh's theory. Furthermore, the amplitude of the first harmonic follows an exponential law according to $A_1(t) = A_0 e^{\sigma t} + \tilde{A}$, which delivers the growth rate σ.

Figure 5(b) shows the evolution of the wavelength of the previously constructed periodic function. We observe a variation of the wavelength in time, which is beyond Rayleigh's theory for a liquid column. There the maximal unstable mode for the case $\nu = 0$ is expected to be situated at $\lambda = 4.51$ mm for our nozzle radius of 0.5 mm. Notwithstanding, the exponential growth of the amplitude remains true. This behaviour is in principle observed for all investigated glycerin–water mixtures.

In figure 6 we have plotted the measured growth rate σ, marked by full circles, versus the kinematic viscosity. The growth rate decays with increasing viscosity. Lacking a specific

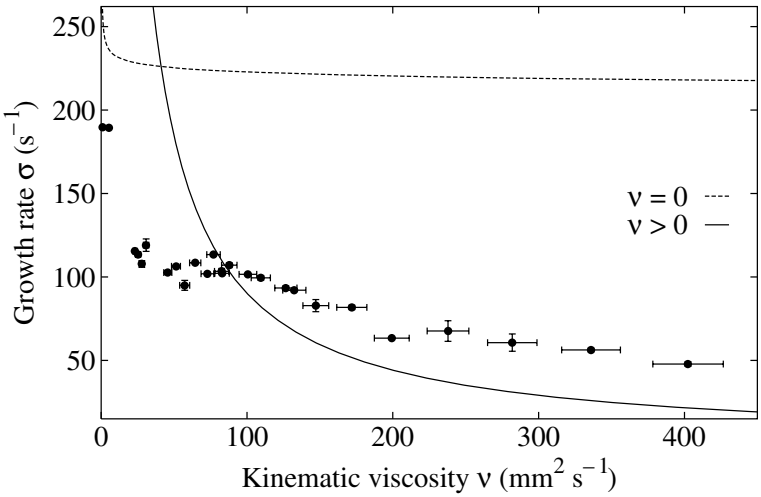

Figure 6. Growth rate as a function of kinematic viscosity. The dashed (solid) curve gives the theoretical expectation without (including) viscosity for the fastest growing mode according to the Rayleigh theory.

theory for the first regime of drop formation we present together with the data the predictions of Rayleigh's theory for $\nu = 0$ ($\nu > 0$) denoted by a dashed (solid) curve. To obtain the dashed curve for $\nu = 0$ we calculate the maximum of the theoretical growth rate σ, which is proportional to a combination of material parameters according to

$$\sigma \sim \left(\frac{\gamma}{\varrho r_0^3}\right)^{1/2}. \tag{1}$$

The material parameters (γ, ϱ, ν) we obtain by appropriate interpolation of tabulated values of the corresponding glycerin–water mixture. Precisely, we use a cubic spline for γ and ρ, and a fourth-order polynomial for $\log(\nu\varrho)$. For comparison, the solid curve shows the growth rates

$$\sigma \sim \frac{\gamma}{\nu\varrho r_0} \tag{2}$$

for the case $\nu > 0$ at that wavenumber where the inviscid theory yields a maximum of the growth rate. The order of magnitude and the tendency for $\nu > 0$ agree. A better agreement can hardly be expected because of the different boundary conditions and the fact that gravity is not included in the theory.

In the following we focus on the time interval immediately before the rupture. Already in figure 4 one can observe a transition from the first, linearly unstable regime (indicated by a solid curve) to the self-similar area (indicated by a dashed line). A more detailed view of the last few milliseconds is presented in figure 7. For a given viscosity the neck radius $h_{\min}$ is shown as a function of time. One can clearly distinguish two different regimes with different shrink velocity.

These regimes have been predicted by theory [8, 11]. The theory yields for the scaling function describing the drop profile a symmetric one for small Reynolds numbers, and an asymmetric one in the later stages of the temporal evolution. As a consequence of the self-similarity the neck radius can be described by

$$h_{\min} = u_{(a)s}\frac{\gamma}{\nu\varrho}(t_0 - t). \tag{3}$$

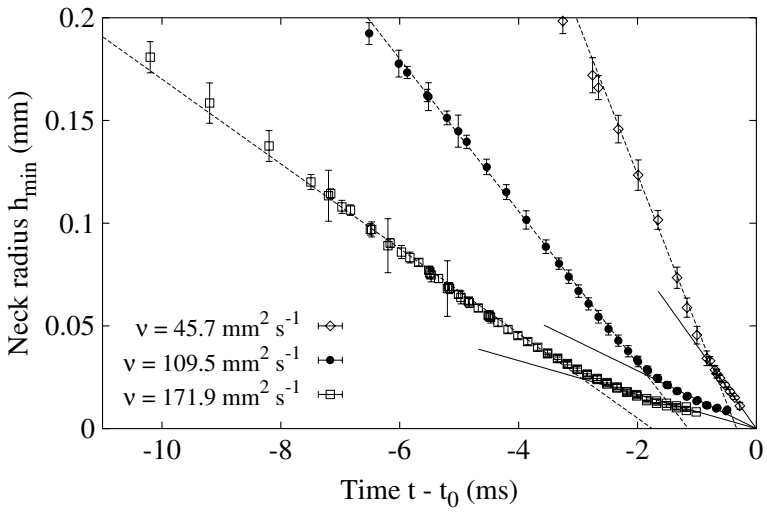

Figure 7. Time evolution of the neck radius in the last stage of the pinch-off. The dashed lines are linear fits according to Stokes flow and the solid ones describe the linear behaviour in the Navier–Stokes regime. Symbols as in figure 4.

Here $u_{(a)s}$ denotes the predicted dimensionless shrink velocities for the case of an (a)symmetric scaling function, respectively. They amount to $u_s = 0.0709$ for the viscous-dominated or Stokes flow [8] and $u_{as} = 0.0304$ for the intertial–viscous or Navier–Stokes flow [11, 6]. In this way one obtains for the shrink velocity in real space the expression

$$v_{(a)s} = u_{(a)s}\frac{\gamma}{\nu\varrho}. \tag{4}$$

The neck of the drop shrinks now with a constant velocity, which scales only with the material parameters.

For a given viscosity the dashed line in figure 7 displays the linear fit according to the Stokes flow. With decreasing neck radius the flow velocity within the neck has to increase and thus inertia can no longer be neglected. So the solution for Stokes flow must give way to the one which includes inertia, i.e. the similarity solution for Navier–Stokes flow. The linear fit according to the latter flow is marked in figure 7 by a solid line.

In each flow regime we clearly observe a decrease of the shrink velocity due to an increase of the viscosity. The shrink velocity obtained by the linear fits is plotted in figure 8 for varying kinematic viscosity. The shrink velocity in the Stokes regime is marked by open squares, and decays rapidly with increasing viscosity. The same is true for the shrink velocity in the Navier–Stokes regime, which is denoted by full circles. The dashed line displays the functional dependence of the shrink velocity according to equation (4) for the Stokes flow, where the variation of all three material parameters (γ, ϱ, ν) under variation of the mass fraction has been taken into account. The solid line gives the corresponding prediction for the Navier–Stokes flow. The offset between the two curves is determined by the difference in the dimensionless shrink velocities $u_{(a)s}$. A remarkably good agreement can be observed for a wide range of viscosities presented here.

So far the experiments have shown that three different flow regimes do indeed exist. Now we focus on the range of existence of these regimes as a function of the viscosity, in order to get hints for the nature of the transition between these different flow types. We start with the

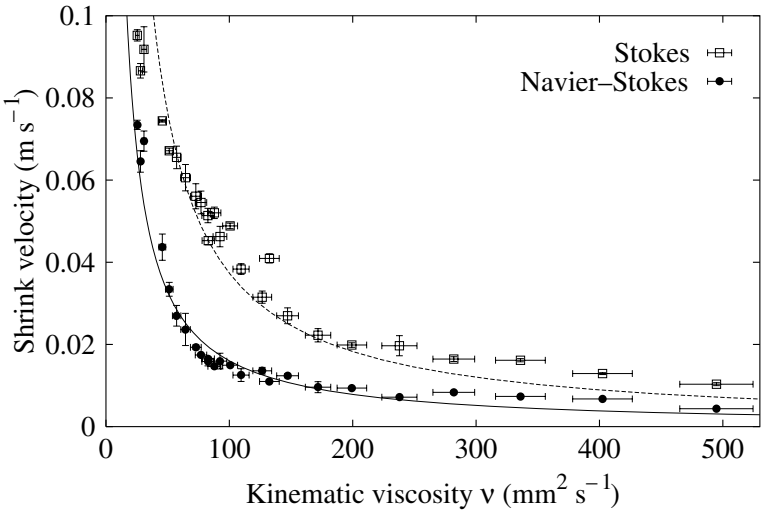

Figure 8. The measured shrink velocity as a function of the kinematic viscosity is shown as open squares (solid circles) for the Stokes (Navier–Stokes) regime and the theoretical expectation by the dashed (solid) curve, respectively.

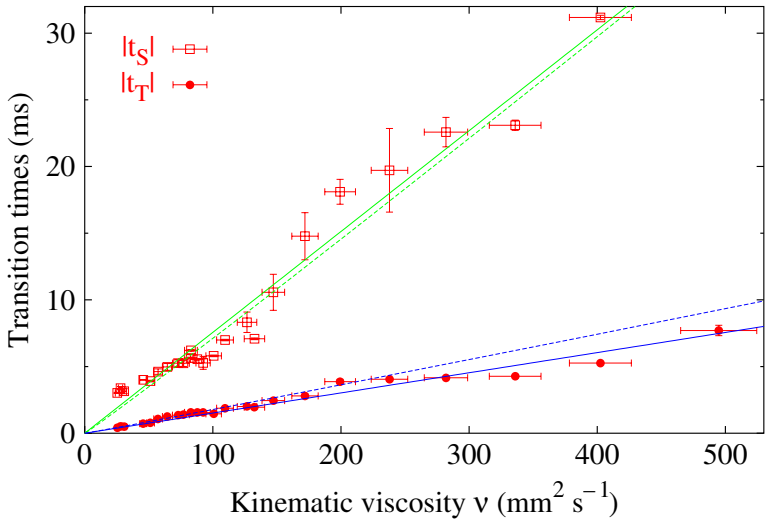

Figure 9. Transition times as a function of kinematic viscosity. The transition time t_S between the accelerating region and the Stokes flow is marked by open squares and the transition point t_T between Stokes flow and Navier–Stokes flow by solid circles, respectively. The solid lines represent best linear fits. The dashed lines mark the phenomenological explanation given in the text.

crossover from accelerated flow to the first self-similar regime. We take the point of intersection of the exponential and the linear function as the transition time t_S between the first two flow types. This quantity is shown by open squares as a function of kinematic viscosity in figure 9. With growing viscosity the values for $|t_S|$ increase, i.e. the flow starts increasingly earlier to behave according to Stokes. The green solid line gives the best linear fit to the data. Moreover, we have determined the transition times t_T between the Stokes and Navier–Stokes regimes by

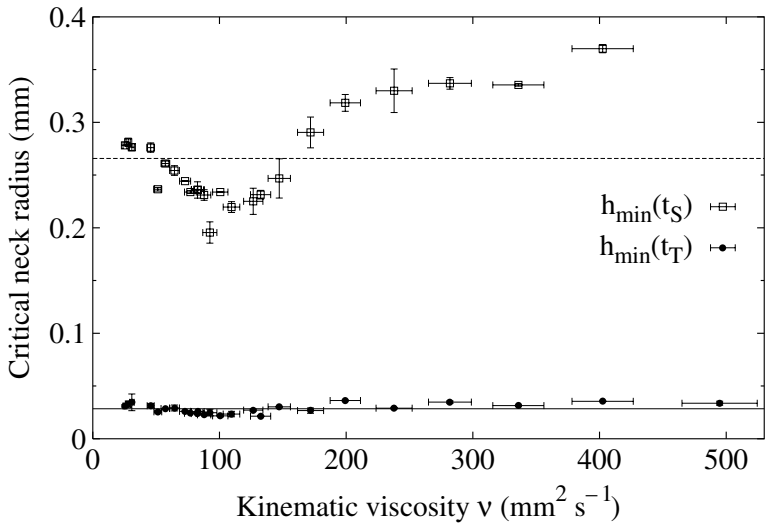

Figure 10. The critical neck radii versus the kinematic viscosity.

the point of intersection of both linear functions in figure 7. The values are marked in figure 9 by full circles. Again $|t_T|$ rises with increasing viscosity. A linear fit is given by the blue solid line.

In figure 10 we show the critical neck radii $h_{min}(t_S)$ and $h_{min}(t_T)$, as extracted from the experimental data. For both quantities we observe small modulations around the average values denoted by the dashed and solid lines, respectively. This cum grano salis constant behaviour is a remarkable fact in itself. For the transition to Stokes flow a critical neck radius $h_{min}(t_S) = 0.27 \pm 0.04$ mm is found in the experiment; for the transition to Navier–Stokes flow $h_{min}(t_T)$ amounts to 28.5 ± 4.4 μm. For comparison, the radius of the nozzle is $r_0 = 0.5$ mm.

From this observation the functional dependence of the transition times can be deduced as follows. Decomposing equation (3) to t_S (where $t_S = t_0 - t$) yields

$$t_S = \frac{\nu\varrho}{\gamma u_s} h_{min}(t_S). \tag{5}$$

In figure 9 this functional dependence is marked by the green dashed line. It can hardly be discriminated from the linear fit given by the solid line. The same holds true for the transition to Navier–Stokes flow:

$$t_T = \frac{\nu\varrho}{\gamma u_{as}} h_{min}(t_T), \tag{6}$$

as marked in figure 9 by the blue dashed line.

Finally, we investigate the Reynolds number at the transition from Stokes- to Navier–Stokes flow. An estimation for the Reynolds number can be obtained as follows. Assuming the velocity inside the neck at the position of its minimum is zero, in the moving reference frame the flow rate at a certain distance z can be written as

$$v(z)h^2(z)\pi = \int_{z_{min}}^{z} \frac{\mathrm{d}h\,(z')}{\mathrm{d}t} 2\pi h(z')\,\mathrm{d}z'. \tag{7}$$

Thus the Reynolds number amounts to

$$Re(z) = \frac{(v(z) + v_{min})z_{min}}{\nu}, \tag{8}$$

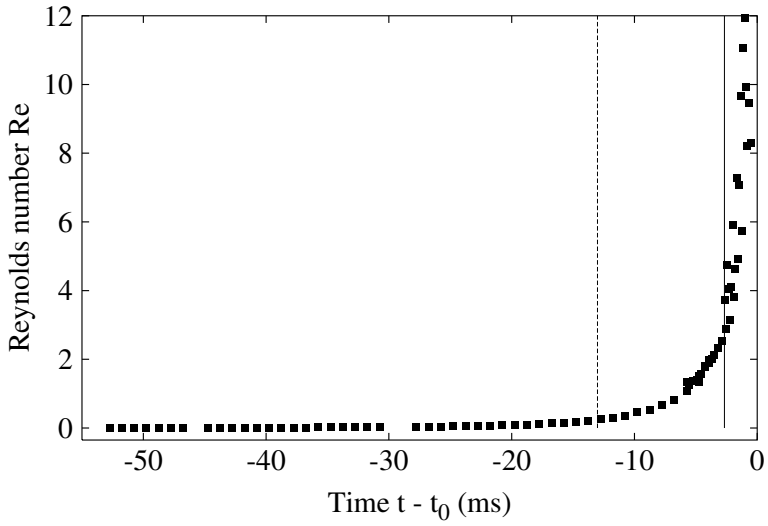

Figure 11. The Reynolds number versus time. The dashed line denotes t_S, and the solid line denotes t_T. For clarity the statistical error has been omitted. The viscosity is $\nu = 171.9\ \mathrm{mm}^2\ \mathrm{s}^{-1}$, which corresponds to the open squares in figures 4 and 7.

where $v(z)+v_{\min}$ gives the flow velocity in the laboratory frame, and $z_{\min}$ the characteristic length in the axial direction. This local Reynolds number $Re(z)$ grows with increasing distance from the neck radius, and typically passes through a maximum. This maximal value will be in the following addressed as the Reynolds number. In figure 11 this quantity is plotted versus time for one set of material parameters.

Starting in the range of 10^{-3} the Reynolds number increases monotonically for four orders of magnitude. The transition from Stokes to Navier–Stokes flow takes place at $Re(t_T) \approx 3$. Thus, so far, the drastic increase of $Re(t)$ for $t > t_T$ is well in agreement with the increasing importance of inertia.

Next, we inspect the viscosity dependence of $Re(t_T)$ as shown in figure 12. Each data point has been determined by averaging three values of $Re(t)$ which are situated nearest to t_T. For growing viscosity $Re(t_T)$ is found to decay rapidly. The solid curve gives a least-square fit according to $Re(t_T) \propto \nu^{\kappa}$ with $\kappa = -1.1 \pm 0.1$. This viscosity dependence is surprising because one could expect that the transition to Navier–Stokes flow takes place at a critical, constant Reynolds number. By definition, the Reynolds number is inversely proportional to viscosity. This reconfirms our earlier observation that the transition to the inertial–viscous flow regime occurs at a constant critical neck radius.

4. Summary and conclusion

In the accelerated flow regime we have observed an exponential evolution of the neck radius. This indicates a linear instability of the pendant drop. However, the behaviour of the wavelength is not in agreement with Rayleigh's theory for a liquid column. In addition, the viscosity dependence of the growth rate is met only in the tendency. Thus, we find, together with Clanet and Lasheras [5], that an exponential growth takes place, and we agree in part with Henderson

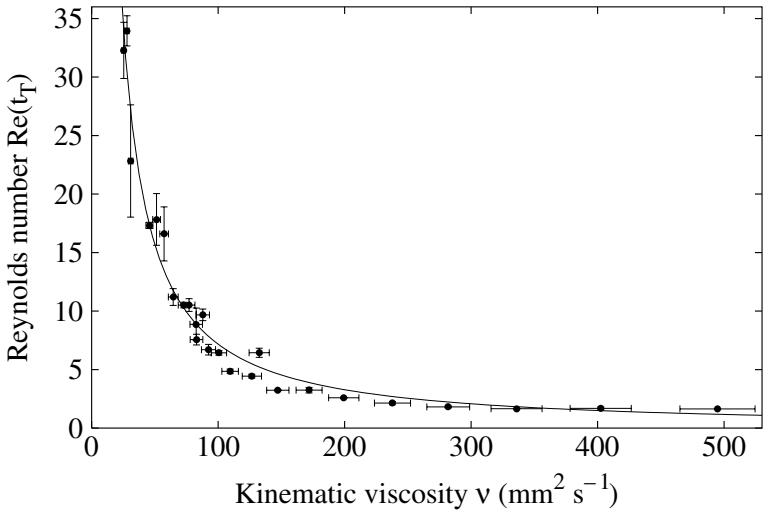

Figure 12. The Reynolds number at the transition time t_T versus the kinematic viscosity.

et al [4] that Rayleigh is not applicable. Unfortunately, to our knowledge no proper analytical description for the pendant drop becoming unstable is available. This may be due to the fact that, in contrast to a liquid column, the initial shape of a pendant drop is strongly dependent on its material parameters and not universal.

In the self-similar flow regime we have seen a quantitative agreement between the theoretical predictions and the experimental data. The temporal evolution of the neck radius and the viscosity dependence of the shrink velocity verify the theoretical predictions. Moreover, we have found an increase of the temporal extension of the Stokes and Navier–Stokes flow, as presented in figure 9. The transition between the latter two regimes has been theoretically suggested in [6, 18]. It has been found in experiment, where an asymmetry parameter served as an order parameter for the transition from a symmetric to an asymmetric profile [14]. However, to our knowledge, theory cannot give an estimate for the time t_T, where the transition takes place. Under variation of the mass fraction we have found a simple functional dependence of both transition times (t_S, t_T) on the material parameters (γ, ϱ, ν). Moreover, it was uncovered that the transitions take place at constant critical neck radii $h_{min}(t_S)$ and $h_{min}(t_T)$. Remarkably, this observation explains via equations (5) and (6) the variation of the transition times with the material parameters.

One might expect that the transition from viscous-dominated to inertial–viscous flow is connected with a certain threshold of the Reynolds number. However, inspecting the viscosity dependence we discover an inversely proportional behaviour. This finding, together with the constant critical neck radius, leaves us with a riddle to be solved by theory. An explanation should include the fact that the transition to viscous flow takes place at a constant radius.

Acknowledgments

The authors thank Th M Bock for technical support, and 'Deutsche Forschungsgemeinschaft' (grant Re588/12) for financial support.

References

[1] Rayleigh J W S 1892 *Phil. Mag.* **34** 145
[2] Donnelly R J and Glaberson W 1966 *Proc. R. Soc.* A **290** 547
[3] Goedde E F and Yuen M C 1970 *J. Fluid Mech.* **40** 495
[4] Henderson D M, Segur H, Smolka L B and Wadati M 2000 *Phys. Fluids* **12** 550
[5] Clanet C and Lasheras J C 1999 *J. Fluid Mech.* **383** 307
[6] Eggers J 1997 *Rev. Mod. Phys.* **69** 865
[7] Peregrine D H, Shoker G and Symon A 1990 *J. Fluid Mech.* **212** 25
[8] Papageorgiou D T 1995 *Phys. Fluids* **7** 1529
[9] Rothert A and Richter R 1999 *J. Magn. Magn. Mater.* **201** 324
[10] Lee H C 1974 *IBM J. Res. Dev.* **18** 364
[11] Eggers J 1993 *Phys. Rev. Lett.* **71** 3458
[12] Kowalewski T A 1996 *Fluid Dyn. Res.* **17** 121
[13] Shi X D, Brenner M P and Nagel S R 1994 *Science* **265** 219
[14] Rothert A, Richter R and Rehberg I 2001 *Phys. Rev. Lett.* **87** 084501
[15] Lechner M D (ed) 1997 *Numerical Data and Functional Relationships in Science and Technology (Landolt–Börnstein)* vol IV/16 (Berlin: Springer)
[16] Schäfer K (ed) 1977 *Zahlenwerte und Funktionen aus Naturwissenschaften und Technik (Landolt–Börnstein)* vol IV/1b (Berlin: Springer)
[17] Lax E (ed) 1967 *Taschenbuch für Chemiker und Physiker (D'Ans–Lax)* vol I (Berlin: Springer)
[18] Lister J R and Stone H A 1998 *Phys. Fluids* **10** 2758